JES Focus Issue on Electrochemical Capacitors: Fundamentals to Applications

Flowable Conducting Particle Networks in Redox-Active Electrolytes for Grid Energy Storage

K. B. Hatzell,[a,*] M. Boota,[a,*] E. C. Kumbur,[b] and Y. Gogotsi[a,,z]**

[a]*A. J. Drexel Nanomaterials Institute, Department of Materials Science and Engineering, Drexel University, Philadelphia, Pennsylvania 19104, USA*
[b]*Electrochemical Energy Systems Laboratory, Department of Mechanical Engineering and Mechanics, Drexel University, Philadelphia, Pennsylvania 19104, USA*

This study reports a new hybrid approach toward achieving high volumetric energy and power densities in an electrochemical flow capacitor for grid energy storage. The electrochemical flow capacitor suffers from high self-discharge and low energy density because charge storage is limited to the available surface area (electric double layer charge storage). Here, we examine two carbon materials as conducting particles in a flow battery electrolyte containing the VO^{2+}/VO_2^+ redox couple. Highly porous activated carbon spheres (CSs) and multi-walled carbon nanotubes (MWCNTs) are investigated as conducting particle networks that facilitate both faradaic and electric double layer charge storage. Charge storage contributions (electric double layer and faradaic) are distinguished for flow-electrodes composed of MWCNTs and activated CSs. A MWCNT flow-electrode based in a redox-active electrolyte containing the VO^{2+}/VO_2^+ redox couple demonstrates 18% less self-discharge, 10 X more energy density, and 20 X greater power densities (at 20 mV s^{-1}) than one based on a non-redox active electrolyte. Furthermore, a MWCNT redox-active flow electrode demonstrates 80% capacitance retention, and >95% coulombic efficiency over 100 cycles, indicating the feasibility of utilizing conducting networks with redox chemistries for grid energy storage.
 [DOI: 10.1149/2.0011505jes]

Manuscript submitted November 3, 2014; revised manuscript received December 19, 2014. Published January 9, 2015. *This paper is part of the JES Focus Issue on Electrochemical Capacitors: Fundamentals to Applications.*

Grid energy storage is a critical component toward the integration of renewable energy technologies and ensuring reliable distribution of electricity.[1,2] Numerous flow-assisted electrochemical systems (FAESs) based on different active materials are being pursued including redox flow batteries (RFB),[3–5] semi-solid flow batteries,[6,7] organic-redox flow batteries,[8–10] and the electrochemical flow capacitor (EFC).[11,12] A flow-architecture provides for scalable and modular systems, decoupled power and energy densities, and a potentially low-cost means for storing energy at the grid level (Fig. 1a).

All FAESs utilize active materials either dissolved in an electrolyte solution or suspended in an electrically conductive flow-electrode for scalable energy storage (Fig. 1). Redox-flow batteries and organic-redox flow batteries both utilize soluble redox species as the active materials (Figs. 1c and 1d). In traditional RFBs, soluble metal ions (vanadium, cerium, iron, etc.) are used, while organic RFBs utilize soluble organic compounds (e.g. quinones) as active material. Metal ions have been widely studied in commercial RFBs and are the closest technology to be widely used. FAESSs based on organic compounds are new and promising for grid energy storage applications because they do not rely on precious metals, have tunable properties based on their chemical structure,[13,14] and have the potential to be low-cost, durable, environmentally friendly, and scalable. Both of these systems rely on chemical reactions based on heterogeneous charge transfer for charge storage. Vanadium compounds have been known to have sluggish kinetics when compared to quinone-based molecules, which undergo rapid two-proton two-electron reactions.[9] For improved reaction kinetics, the RFB research community has looked into optimizing the electrode|solution interface for improved convection processes, and decreased kinetic, ohmic, and transport losses.[3,15,16] Toward this goal, several electrode architectures are being examined including: flow-by, flow-through, and interdigitated flow field configurations.[15,16] A fourth architecture, semi-solid flow-electrodes, has yet to be reported in the RFB community, and is the subject of this work (Fig. 1b).

Semi-solid flow-electrodes are electronically conductive with a solid active material suspended in the electrolyte (Fig. 1e and 1f). There are two families, ones that utilize intercalation materials for faradaic energy storage[17,18] (semi-solid flow battery), and ones that utilize porous carbon for electrostatic energy storage in an electric double layer (flow capacitor with capacitive suspension electrodes).[11,19–22] The use of a energy dense intercalation compound ($LiFePO_4$) in organic electrolytes has shown excellent results demonstrating large voltage windows and high charge storage capacity when compared to traditional aqueous RFBs. Nevertheless, there are challenges with working in non-aqueous environments and achieving satisfactory power performance (discharge rate). In contrast, the EFC utilizes low-cost, and abundant materials such as porous carbon, as the active component in aqueous solutions,[21,23] but suffers from low energy density because energy storage is limited to the available surface area. Capacitive suspension electrodes are also strong candidates for low-energy, low-concentration ion removal in applications such as capacitive deionization (desalination) and capacitive mixing (energy generation) and benefit from fast ion adsorption processes.[24–29] Nevertheless, for success in energy storage applications, self-discharge and energy density issues need to be addressed. Previously, this energy density issue has been addressed by hybridizing the EFC with either redox-active organic molecules,[23] or pseudocapacitive metal-oxides,[21] e.g. MnO_2.

Here, we present another hybrid approach, where we combine a carbon-based semi-solid flow-electrode with a common redox active electrolyte containing the VO^{2+}/VO_2^+ redox couple with the goal of enhancing the volumetric energy density through the combination of electric double layer and faradaic charge storage mechanisms and mitigating self-discharge processes.[30,31] The SSFE acts as a conducting network for greater percolation regions, beyond the electrode surface. Recently, Fan et al. demonstrated that the addition of conducting particles in a flow-battery solution increased the charge transfer region and decreased the diffusion lengths in a polysulfide flow battery (Fig. 1b).[7,32] Here, we have expanded upon this concept, and examined two types of carbon materials as nanoscale (multi-walled carbon nanotubes (MWCNTs)) and micro-scale (activated carbon spheres (CSs)) conductive particles in an aqueous electrolyte. In this preliminary

*Electrochemical Society Student Member.
**Electrochemical Society Fellow.
zE-mail: gogotsi@drexel.edu

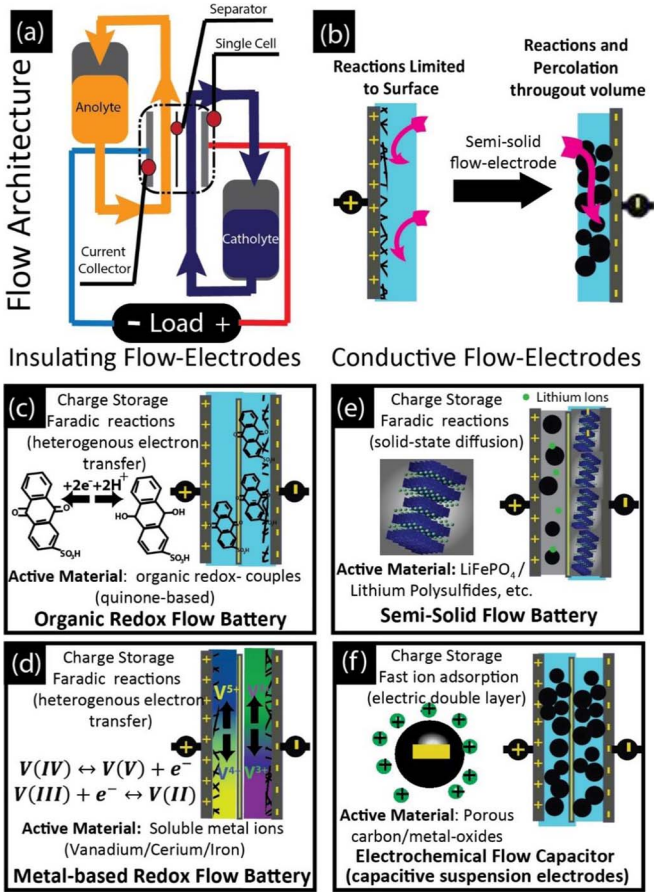

Figure 1. Summary of flow-assisted electrochemical systems that utilize flowable architectures (a) for large-scale electrochemical energy storage. Flow-electrodes allow for percolation networks for more reaction sites per volume of electrolyte (b). Organic flow batteries (c) and metal-based redox flow batteries (d) are two examples of flow systems that operate with electrically insulating liquids. The semi-solid flow battery utilizes intercalation compounds, which are energy-dense materials, for high energy density energy storage (e), whereas flow capacitors utilize high surface area (highly porous) materials and electric double layer charge storage for high power grid applications and desalination (f).

study, we chose to examine the most traditional redox electrolyte based on the $VO^{2+}/VO_2{}^{+}$ redox couple to achieve a baseline for the reaction kinetics in different carbon percolation networks.

Experimental

Flow-electrode preparation.— Four flow-electrodes were examined in this study. Two flow-electrodes used MWCNTs as the flowable substrate. Two used high surface area CSs as the flowable substrate. Two different electrolytes were used as the flow solutions in this study: 4 M H_2SO_4, and 1 M vanadium (IV) oxide sulfate hydrate ($VOSO_4 \cdot xH_2O$, Sigma Aldrich) dissolved in 4 M H_2SO_4 solutions (Fischer Scientific).

MWCNTs (Arkema, France) containing flow electrodes were prepared by mixing the 4 M H_2SO_4 solution, and 1 M $VOSO_4$/4M H_2SO_4 with MWCNTs. Both flow-electrodes had a gravimetric ratio of 1:10 (solid:liquid). MWCNTs containing flow-electrodes were compared with flow electrodes made of CSs derived from phenolic resins (MAST Carbon, United Kingdom).[19,33] The CS-based flow-electrodes were studied in same electrolytes (4 M H_2SO_4 and 1 M $VOSO_4$/4M H_2SO_4) at a gravimetric ratio (solid:liquid) of 1:4. Before combining electrolytes and solid materials, the electrolytes were purged with argon for about 1 hour to eliminate traces of oxygen. It should be noted that the amounts of carbon added (4:1 for CSs and 10:1 for MWCNTs weight ratio) were selected to keep the overall densities of the flow-electrodes similar (CS ~0.40 g/mL and MWCNT ~0.15 g/mL).

Electrochemistry measurements.— All tests were performed in a two-electrode static configuration. The self-manufactured cell used for the electrochemistry experiments was composed of two stainless steel current collectors with 610 μm channels designated by latex gaskets as described by previous work.[19,21] For comparison, all electrodes studied were 85 mg (electrolyte+carbon materials). Each symmetric cell was separated by a Nafion 117 membrane (Fuel Cell Etc., USA) with an effective area of 1 cm^2. All Nafion 117 membranes were pretreated prior to use at 75°C for 1 h in 3% hydrogen peroxide, 1 h in deionized water, 1 h in 0.5 M sulfuric acid, and finally 1 h in deionized water. Membranes were stored throughout all experiments in deionized water.

Electrochemical measurements were performed at room temperature on a VMP3 potentiostat/galvanostat (BioLogic, France). Cyclic voltammetry (CV) was carried out at 2, 5, 10, and 20 $mV \cdot s^{-1}$ sweep rates. From CV, the specific gravimetric capacitance (C_{sp}) was derived using the following equation:

$$C_{sp} = \left(\frac{2}{\Delta E} \cdot \frac{\int i dV}{v \cdot m}\right), \quad [1]$$

where ΔE is the width of the voltage window, i is the discharge current, V is the voltage, v is the sweep rate, and m is the mass of carbon in one electrode. The factor of two accounts for the two-electrode setup.[34] Galvanostatic cycling was completed for assessment of lifetime, coulombic, voltage and energy efficiencies. The coulombic efficiency was calculated by Eq. 2:

$$\eta_c = \frac{\int_{discharge} I dt}{\int_{charge} I dt} \quad [2]$$

and is the ratio between the discharge capacity and charge capacity. The voltage efficiency (η_v) was taken to be the ratio of the discharge voltage to charge voltage during galvanostatic cycling. Finally, the energy efficiency was calculated as:

$$\eta_e = \eta_c * \eta_v \quad [3]$$

Each suspension electrode was tested with potentiodynamic electrochemical impedance spectroscopy (PEIS) to understand how to characterize the potential of chemical reactions and flow-electrode conductivity. The ohmic resistance of the static cell, R_Ω, was determined from the impedance spectrum intersection with the real axis and was compared for the electrodes composed of MWCNTs and CSs and for each electrolyte. The area specific resistance (ASR) was reported by multiplying the ohmic resistance by the flow-electrode cross-sectional area. All spectra were run in the frequency range of 200 kHz to 100 mHz at a sine wave signal amplitude of 10 mV and each voltage between 0.1–1.4 ($\Delta V = .1$ V).

CV at rates ranging from 2 to 20 $mV\ s^{-1}$ were used to distinguish quantitatively the capacitive and the faradaic (diffusion limited) charge storage contributions. A procedure similar to the one described by Wang et al. was followed.[35–37] In capacitive systems, charge storage is dominated by ion adsorption at the surface of a material via electrostatic forces. In this process, the current is proportional to the sweep rate. In contrast, in systems that utilize faradaic charge storage mechanism (diffusion-limited process), the current is proportional to the square root of the sweep rate. The current response of a CV can be partitioned into capacitive and faradaic charge storage by approximating the current as:

$$i(V) = k_1 v + k_2 v^{\frac{1}{2}} \quad [4]$$

In equation 4, $k_1 v$ is the current contribution from electric double layer charge storage processes, and $k_2 v^{\frac{1}{2}}$ is representative of diffusion-limited charge storage. To determine k_1, and k_2, a plot of the current

response at each voltage normalized to the square root of the sweep rate was plotted:

$$\frac{i\,(V)}{v^{\frac{1}{2}}} = k_1 v^{-\frac{1}{2}} + k_2 \qquad [5]$$

and fitted with a line.

Results and Discussion

Figure 2 demonstrates the effect of adding soluble redox species into the electrolyte in a flow-electrode based on low surface area materials (MWCNTs) (Figs. 2a and 2c) and high-surface area (porous activated CSs) (Figs. 2b and 2d). MWCNTs as a substrate for a flow-electrode in sulfuric acid demonstrates pseudo-polarizable behavior (Fig. 2a). At low potentials, an increase in current is observed as a result of oxidation reactions. It should be noted that these 'bumps' were more pronounced (at 0.9 V and 0 V) when the electrolyte was not bubbled with argon prior to experiments. The slope of *V/I* at 0.9 V is nearly zero (across all rates), indicating a very small resistance, high rate handling, and good conductivity for ion percolation. Nevertheless, the current is low because there is no redox species, and charge storage is primarily electrostatic (electric double layer). The addition of VO_2^+ species in the case of 1 M $VOSO_4$/4 M H_2SO_4 electrolyte results in pronounced redox peaks at ~0.45 V (cathodic) and 0.9 V (anodic) both at 2 mV s^{-1} (Fig. 2c). As the sweep rate increases the distance between the anodic and cathodic peaks also increases, which means the reversibility of the vanadium oxidation/reduction reaction decreases in the percolation network formed by the MWCNTs. There are several popular strategies reported in the literature including oxidation of the active material, and/or the addition of electrocatalytic nanoparticles for more facile kinetics.[38,39] Nevertheless, the presence of pronounced redox peaks demonstrates the utility of MWCNTs as the conductive material for redox electrolytes.

For the highly porous carbon spheres (CSs) in 4 M H_2SO_4, an increase in current is observed when compared with MWCNTs (Fig. 2a vs. 2b). The increase in current is because the CSs have a significantly greater specific surface area (~1600 m^2 g^{-1} compared to ~200 m^2 g^{-1} for MWCNTs), and without the presence of soluble redox species, the charge storage is limited to EDL (H^+ or SO_4^{2-} adsorption on the carbon surface). Nevertheless, when a redox couple is added to the electrolyte based on CSs, no pronounced peaks are observed (Fig. 2d). The CV is distorted from the pseudo-rectangular shape apparent in the flow-electrode based on CSs in 4 M H_2SO_4 and the current is slightly higher indicating additional contributions to charge storage (faradaic reactions). The results indicate that faradaic charge storage is less pronounced in the flow-electrode based on highly porous CSs. Both suspension electrodes based on a redox-active electrolyte have an expanded voltage window (1.2 and 1.4 V). Thus, both systems have enhanced energy densities, when compared to systems based on a 0.9 V voltage window (commonly seen in H_2SO_4 based systems). To increase the voltage window (and energy densities) even further, organic electrolyte systems are being explored.[40]

The conducting carbon network can serve in two roles:[1] catalyst and interface for additional and simultaneous oxidation and reduction reactions throughout the electrode volume, and[2] a source for EDL charge storage. Carbon materials (especially when highly conductive and porous) can adsorb ions and store charge. This phenomenon is apparent in the CVs (Figs. 2a and 2b). The addition of a redox couple (VO^{2+}/VO_2^+) into the electrolyte adds another charge storage mechanism (faradaic). Fig. 3 gives a breakdown for the total charge storage in MWCNT flow-electrode (Figs. 3a and 3b) and CS flow-electrode (Figs. 3d and 3e) with a VO^{2+}/VO_2^+ redox couple at 2 mV s^{-1} and 20 mV s^{-1}. The cross-hatched regions represent the EDL charge storage, while the remaining area corresponds to diffusion-controlled processes, such as chemical reactions associated with the VO^{2+}/VO_2^+ redox couple. When the sweep rate is increased, both samples exhibit increased EDL contributions, because diffusion challenges hinder the full utilization of the redox active material (VO^{2+}/VO_2^+). The MWCNT flow-electrode demonstrates greater changes in EDL charge storage contribution between 2 mV s^{-1} and 20 mV s^{-1} (Fig. 3c). The

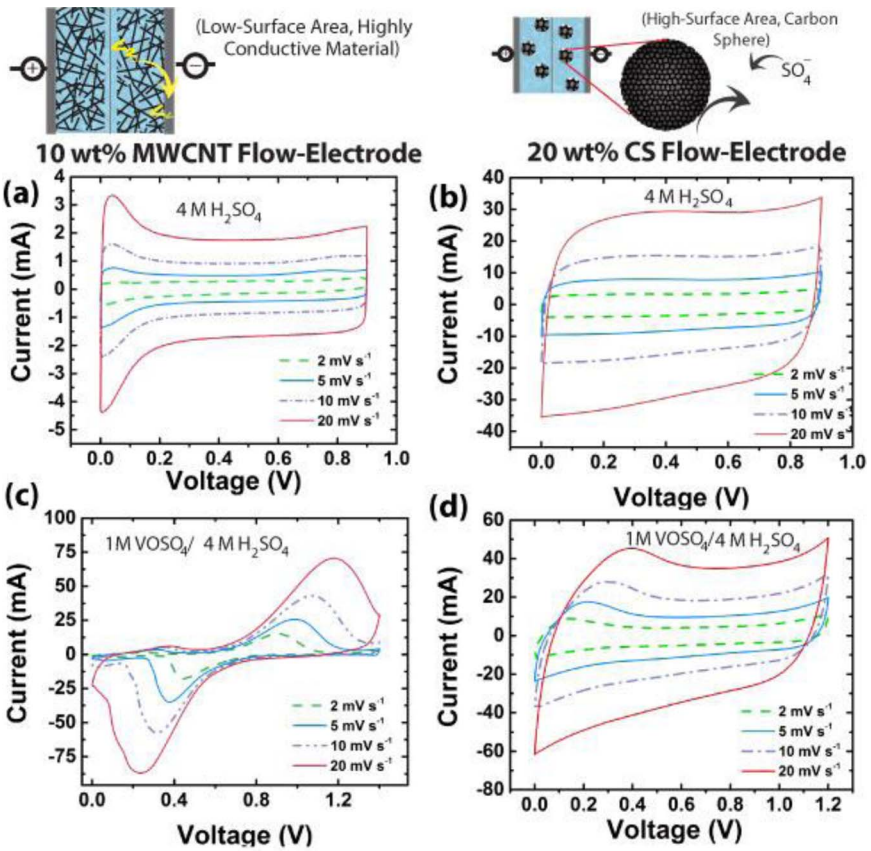

Figure 2. Cyclic voltammograms for flow-electrodes based on nanoscale (MWCNTs) (a) and microscale (CSs) conductive carbon particles (b) in sulfuric acid. CVs are transformed when a VO^{2+}/VO_2^+ redox couple is introduced into the flow-electrodes based on MWCNTs (c) and CSs (d).

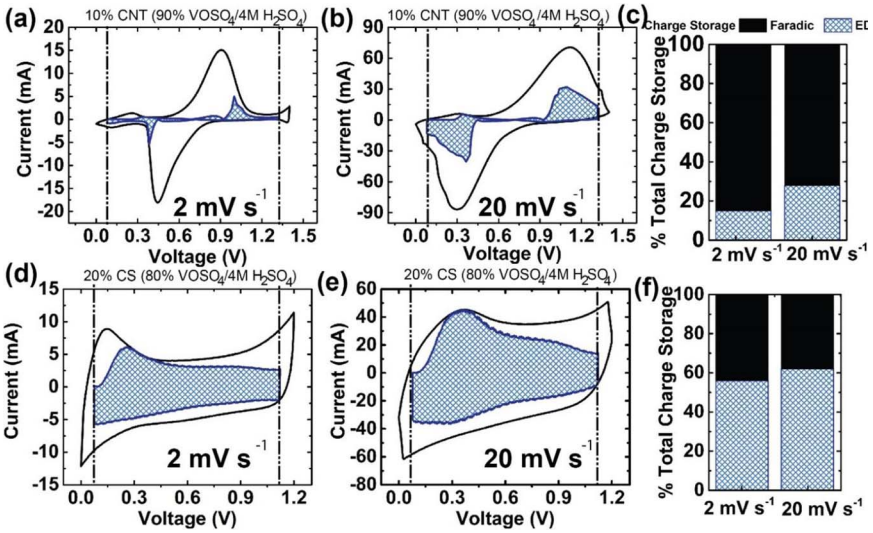

Figure 3. Charge storage contributions for flow-electrodes based on $VO^{2+}/VO_2{}^+$ redox couple in a MWCNT flow-electrode at 2 mV s^{-1} (a) and 20 mV s^{-1} (b) and in a CS flow-electrode at 2 mV s^{-1} (d) and 20 mV s^{-1} (e). The total breakdown for charge storage contributions (faradaic and electric double layer) for the MWCNT flow-electrode (c) and the CS flow-electrode (f) demonstrates the effect of conductor material on energy storage properties. Note: The hashed regions are estimates of electric double layer charge storage.

EDL charge storage nearly doubles from ~15% to 30%, while the CS flow electrode only increases from ~56% to ~62%. The values for EDL and diffusion-related charge storage mechanisms are estimates obtained using the partition method described within the electrochemistry methods section. It should be noted, that the EDL (hatched region) is typically represented by peak currents that are independent of voltage. Here, the non-rectangular region is a function (and limitation) of the analytical analysis and occurs because the peak voltages of the suspension electrodes based on redox-active material, do not occur at the same potential (irreversible behavior). Nevertheless, the EDL contribution is significantly different between suspension electrodes based on MWCNTs and CSs. The addition of carbon-based conductor materials (and EDL charge storage mechanisms) may be an avenue for addressing rate handling and power delivery challenges associated with traditional RFBs which are diffusion limited.

Fig. 4a demonstrates the characteristic shapes of the cathodic region of CVs based on MWCNT and CS flow-electrodes. As discussed previously, the MWCNTs exhibit more pronounced peaks at set potentials, which is characteristic of oxidation and reduction processes ($VO^{2+}/VO_2{}^+$). In order to examine the ongoing faradaic processes (chemical reactions) occurring during charging, electrochemical impedance spectra (highlighted by red circles in Fig. 4a) were recorded at different potentials. Fig. 4b demonstrates characteristic Nyquist plots for a MWCNTs flow-electrode and Fig. 4c demonstrates the Nyquist plot for CS-based flow electrode (Fig. 4c). Each spectrum intersected the x-axis at the same location for an area series resistance (ASR) of ~0.4 $\Omega \cdot cm^2$ for the MWCNT flow-electrode and ~0. 8 $\Omega \cdot cm^2$ for the CS flow-electrode. The low-frequency region of the Nyquist plot for the MWCNT flow-electrode evolves with potential (Fig. 4b). At low potentials, the low-frequency region demonstrates a nearly-vertical tail (characteristic of EDL charge storage). At 0.7 V and 0.9 V, the low frequency region is expanded and displays a ~45° line (inset) which indicates the existence of diffusion limitations. These potentials clearly align with the peak current on Fig. 4a, further demonstrating the presence of vanadium-ions at different oxidation states. In contrast, the CS flow-electrode's Nyquist plots are similar across all potentials (Fig. 4c). There is a small semicircle in the high-frequency region, and then a vertical tail in the low-frequency region. The vertical tail is characteristic of 'capacitive' charge storage. This supports what we observed, when we partitioned the charge storage mechanisms in Figs. 3c and 3d, that the CSs had a significant contribution of EDL charge storage. The highly porous nature of the CSs may actually hinder the full utilization of the redox active electrolyte. The surface area associated with the micropores may not be accessible to the large vanadium ions (thus depleting electrochemically active material) or there may be competitive interactions between ion adsorption and oxidation reactions, which may also lead to underutilization of the electrolyte. Thus, careful design of carbon-based conductors (mesoporous and/or open frameworks) is necessary in order for high utilization of redox electrolytes in a flow-electrode.

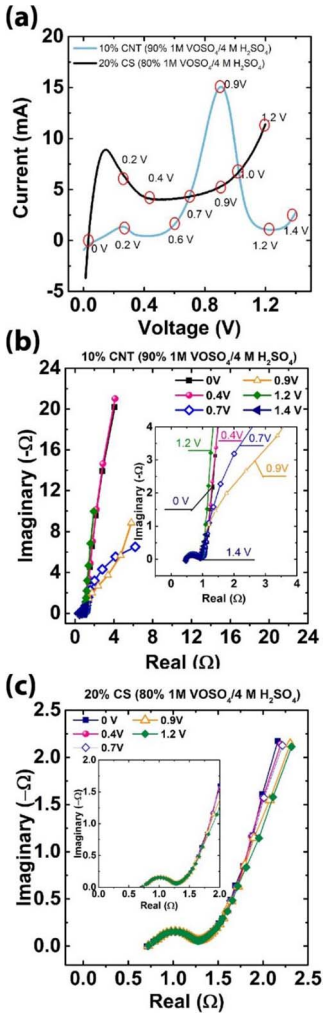

Figure 4. Representative shapes of cathodic curves at 2 mV s^{-1} for flow electrodes based on the $VO^{2+}/VO_2{}^+$ redox couple (a). PEIS at different voltages for the MWCNT (b) and CS (c) based flow-electrodes.

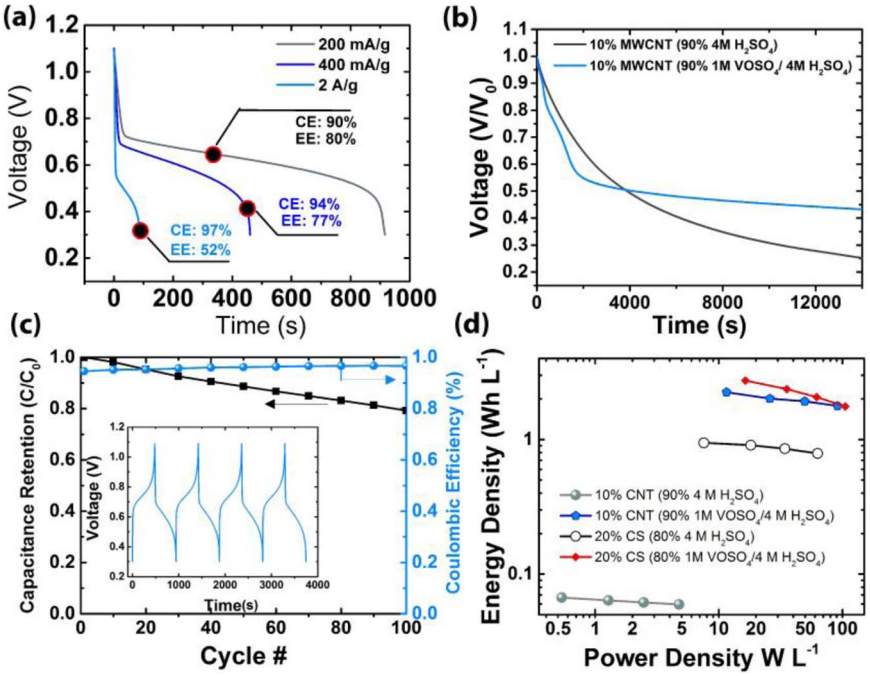

Figure 5. Representative galvanostatic discharge curves at different rates (a), self-discharge (b), cycle life, and coulombic efficiencies at a charge rate of 400 mA g^{-1} (c), and Ragone plot from cyclic voltammetry data in Fig. 2 (d).

Typical galvanostatic discharge curves of the MWCNT flow-electrode at 200 mA g^{-1}, 400 mA g^{-1}, and 2 A g^{-1} current densities are displayed in Fig. 5a. At 200 mA g^{-1} the CE, and EE are 90% and 80%, and at 400 mA g^{-1} the CE and EE are 94% and 77% respectively. A significant decrease in voltage efficiency is observed at the high discharge rate of 2 A g^{-1}, which can be attributed to polarization losses in the cell and slow reaction kinetics. One benefit of these faradaic processes is a notable decrease in self-discharge (Fig. 5b). MWCNTs based in 4 M H_2SO_4 demonstrated a 75% decrease in voltage over 4 hrs while the redox active electrolyte only experienced a decline of 57% (Fig. 4b). Moreover, cycling the MWCNT flow-electrode in the window of 0.3–1.1 V at 400 mA g^{-1} demonstrated 80% overall capacitance (faradaic+capacitive) retention over 100 cycles (Fig. 5c). These preliminary results seem promising because from a material perspective there are several methods to enhance the kinetics of surface reactions via surface modification. Moreover, over the 100 cycles, the coulombic efficiency stays above 95%. Fig. 5d is a Ragone plot comparing the volumetric energy and power densities over the rates of 2 mV s^{-1} to 20 mV s^{-1}. Energy and power densities of ~2 Wh L^{-1} at ~100 W L^{-1} are achieved at a rate of 20 mV s^{-1}. It should be noted that these values are normalized to the entire volume of the SSFE (electrolyte+carbon) and thus represent a conservative estimate. Moreover, only one redox-couple was introduced in this concept study as a control, so it is expected than an asymmetric study with two redox couples would yield even higher energy densities (and an expanded voltage window). Nevertheless, the power densities are significant for the redox chemistry (VO^{2+}/VO_2^+) and further indicate that the increase in volumetric activity sites, may be a method for achieving increased performance in a range of metal-ion based flow battery systems.

Conclusions

The electrochemical performance of two carbon-based conductive networks (flow-electrodes) in a redox-active electrolyte has been investigated for electrochemical flow capacitor applications. The redox activity of VO^{2+}/VO_2^+ is directly tied to the morphology and physical properties of the carbon particles. It was observed that a highly porous carbon (carbon spheres) demonstrated decreased utilization of the electrochemical active ions, which could be tied to the actual accessible surface area of the carbon, or competitive kinetics with ion adsorption processes. Moreover, we report the role of the conducting network on increasing charge storage through EDL contribution, and find that in a MWCNT based electrode, there is a significant increase in charge storage through EDL with increasing scan rates (2 times). A conducting network based on MWCNTs in an electrochemically active solution (VO^{2+}/VO_2^+) demonstrated an increase of 10 X in energy density, nearly a 20 X increase in power density, and a decrease in self-discharge when compared to the solution without the redox couple.

In summary, results of this study support the viability of using a conducting network with metal-ion based chemistries as way to increase the volume in which redox process occur beyond the electrode|solution interface. This approach can be readily adaptable to other redox-flow chemistries, and may be a framework for the realization and utilization of more cost and environmentally friendly metal-ion based systems such as an all-iron flow battery or an organic flow system.

Acknowledgments

The authors acknowledge the support from Fluid Interface Reactions, Structures and Transport (FIRST) Center, an Energy Frontier Research Center funded by the U.S. Department of Energy, Office of Science, Office of Basic Energy Sciences and the National Science Foundation (Grant# 1351161). K.B.H. was supported by the NSF Graduate Research Fellowship (Grant# 1002809).

References

1. B. Dunn, H. Kamath, and J.-M. Tarascon, *Science*, **334**, 928 (2011).
2. Z. Yang, J. Zhang, M. C. Kintner-Meyer, X. Lu, D. Choi, J. P. Lemmon, and J. Liu, *Chemical Reviews*, **111**, 3577 (2011).
3. A. Z. Weber, M. M. Mench, J. P. Meyers, P. N. Ross, J. T. Gostick, and Q. Liu, *Journal of Applied Electrochemistry*, **41**, 1137 (2011).
4. M. Skyllas-Kazacos, M. Chakrabarti, S. Hajimolana, F. Mjalli, and M. Saleem, *Journal of the Electrochemical Society*, **158**, R55 (2011).
5. M. Skyllas-Kazacos, M. Rychcik, R. G. Robins, A. Fane, and M. Green, *Journal of the Electrochemical Society*, **133**, 1057 (1986).
6. M. Duduta, B. Ho, V. C. Wood, P. Limthongkul, V. E. Brunini, W. C. Carter, and Y.-M. Chiang, *Advanced Energy Materials*, **1**, 511 (2011).
7. F. Fan, W. Woodford, Z. Li, N. Baram, K. C. Smith, A. Helal, G. H. McKinley, W. C. Carter, and Y.-M. Chiang, *Nano letters*, **14** 2210 (2014).
8. B. Huskinson, M. P. Marshak, C. Suh, S. Er, M. R. Gerhardt, C. J. Galvin, X. Chen, A. Aspuru-Guzik, R. G. Gordon, and M. J. Aziz, *Nature*, **505**, 195 (2014).

9. B. Yang, L. Hoober-Burkhardt, F. Wang, G. S. Prakash, and S. Narayanan, *Journal of The Electrochemical Society*, **161**, A1371 (2014).
10. F. R. Brushett, J. T. Vaughey, and A. N. Jansen, *Advanced Energy Materials*, **2**, 1390 (2012).
11. V. Presser, C. R. Dennison, J. Campos, K. W. Knehr, E. C. Kumbur, and Y. Gogotsi, *Advanced Energy Materials*, **2**, 895 (2012).
12. S. Porada, J. Lee, D. Weingarth, and V. Presser, *Electrochemistry Communications*, **48**, 178 (2014).
13. S. E. Burkhardt, M. A. Lowe, S. Conte, W. Zhou, H. Qian, G. G. Rodríguez-Calero, J. Gao, R. G. Hennig, and H. D. Abruña, *Energy & Environmental Science*, **5**, 7176 (2012).
14. K. Hernández-Burgos, S. E. Burkhardt, G. G. Rodríguez-Calero, R. G. Hennig, and H. D. Abruña, *The Journal of Physical Chemistry C*, **118**, 6046 (2014).
15. R. M. Darling and M. L. Perry, *Journal of The Electrochemical Society*, **161**, A1381 (2014).
16. D. Aaron, Q. Liu, Z. Tang, G. Grim, A. Papandrew, A. Turhan, T. Zawodzinski, and M. Mench, *Journal of Power sources*, **206**, 450 (2012).
17. M. Duduta, B. Ho, V. C. Wood, P. Limthongkul, V. E. Brunini, W. C. Carter, and Y. M. Chiang, *Advanced Energy Materials*, **1**, 511 (2011).
18. K. C. Smith, Y.-M. Chiang, and W. C. Carter, *Journal of The Electrochemical Society*, **161**, A486 (2014).
19. J. Campos, M. Beidaghi, K. B. Hatzell, C. Dennison, V. Presser, E. C. Kumbur, and Y. Gogotsi, *Electrochimica Acta*, **98**, 123 (2013).
20. M. Boota, K. Hatzell, M. Beidaghi, C. Dennison, E. Kumbur, and Y. Gogotsi, *Journal of The Electrochemical Society*, **161**, A1078 (2014).
21. K. B. Hatzell, L. Fan, M. Beidaghi, M. Boota, E. Pomerantseva, E. C. Kumbur, and Y. Gogotsi, *ACS Applied Materials & Interfaces*, **6**, 8886 (2014).
22. C. Zhang, K. B. Hatzell, M. Boota, B. Dyatkin, M. Beidaghi, D. Long, W. Qiao, E. C. Kumbur, and Y. Gogotsi, *Carbon*, **77**, 155 (2014).
23. K. B. Hatzell, M. Beidaghi, J. W. Campos, C. R. Dennison, E. C. Kumbur, and Y. Gogotsi, *Electrochimica Acta*, **111**, 888 (2013).
24. S.-I. Jeon, H.-R. Park, J.-G. Yeo, S. Yang, C. H. Cho, M. H. Han, and D.-K. Kim, *Energy & Environmental Science*, **6**, 1471 (2013).
25. S.-I. Jeon, J.-S. Park, J.-G. Yeo, S. Yang, J. Choi, and D. K. Kim, *Journal of Materials Chemistry A*, **2**, 6378 (2014).
26. K. B. Hatzell, E. Iwama, A. Ferris, B. Daffos, K. Urita, T. Tzedakis, F. Chauvet, P.-L. Taberna, Y. Gogotsi, and P. Simon, *Electrochemistry Communications*, **43**, 18 (2014).
27. S. Porada, D. Weingarth, H. V. Hamelers, M. Bryjak, V. Presser, and M. Biesheuvel, *Journal of Materials Chemistry A*, **2**, 9313 (2014).
28. Y. Gendel, A. K. E. Rommerskirchen, O. David, and M. Wessling, *Electrochemistry Communications*, **46**, 152 (2014).
29. M. Hatzell, K. B. Hatzell, and B. E. Logan, *Environmental Science & Technology Letters*, **12**, 474 (2014).
30. B. Wang, J. Maciá-Agulló, D. Prendiville, X. Zheng, D. Liu, Y. Zhang, S. Boettcher, X. Ji, and G. Stucky, *Journal of The Electrochemical Society*, **161**, A1090 (2014).
31. E. Frackowiak, K. Fic, M. Meller, and G. Lota, *ChemSusChem*, **5**, 1181 (2012).
32. Y. Yang, G. Zheng, and Y. Cui, *Energy & Environmental Science*, **6**, 1552 (2013).
33. K. B. Hatzell, M. Beidaghi, J. W. Campos, C. R. Dennison, E. C. Kumbur, and Y. Gogotsi, *Electrochimica Acta*, **111**, 888 (2013).
34. M. D. Stoller and R. S. Ruoff, *Energy & Environmental Science*, **3**, 1294 (2010).
35. K. Brezesinski, J. Wang, J. Haetge, C. Reitz, S. O. Steinmueller, S. H. Tolbert, B. M. Smarsly, B. Dunn, and T. Brezesinski, *Journal of the American Chemical Society*, **132**, 6982 (2010).
36. J. Wang, J. Polleux, J. Lim, and B. Dunn, *The Journal of Physical Chemistry C*, **111**, 14925 (2007).
37. T. C. Liu, W. Pell, B. Conway, and S. Roberson, *Journal of the Electrochemical Society*, **145**, 1882 (1998).
38. B. Li, M. Gu, Z. Nie, Y. Shao, Q. Luo, X. Wei, X. Li, J. Xiao, C. Wang, and V. Sprenkle, *Nano letters*, **13**, 1330 (2013).
39. Z. González, A. Sanchez, C. Blanco, M. Granda, R. Menéndez, and R. Santamaria, *Electrochemistry Communications*, **13**, 1379 (2011).
40. R. M. Darling, K. G. Gallagher, J. A. Kowalski, S. Ha, and F. R. Brushett, *Energy & Environmental Science*, **7**, 3459 (2014).